Stress relaxation of dense spongy-particle systems

Stress relaxation of dense spongy-particle systems

Monica E. A. Zakhari*

Polymer Technology, Department of Mechanical Engineering,

Eindhoven University of Technology, P.O. Box 513,

5600 MB Eindhoven, The Netherlands and

Dutch Polymer Institute (DPI), P.O. Box 902,

5600 AX, Eindhoven, The Netherlands

Markus Hütter† and Patrick D. Anderson‡

Polymer Technology, Department of Mechanical Engineering,

Eindhoven University of Technology, P.O. Box 513,

5600 MB Eindhoven, The Netherlands

(Dated: March 23, 2018)

Abstract

Spongy particles have a permeable structure that allows them to undergo rate-dependent volume changes as their elastic network takes up or expels the viscous suspending solvent. Their ability to be jammed well above random close-packing makes them particularly attractive in applications where tailoring the overall properties is a requirement such as, pharmaceuticals and foods. In this work, we independently vary the particle modulus and the particle permeability to study their effect on the stress-relaxation behavior of jammed permeable-particle suspensions. The dynamic two-scale model developed by Hütter et al. [Faraday Discuss., **158**, 407-424 (2012)], which explicitly accounts for the particle size dynamics, is used for this purpose. We perform flow-cessation simulations of dense permeable-particle systems subjected to different pre-shear deformations. The stress relaxation occurs on shorter time scales in the case of permeable particles compared to impermeable particles. In terms of particle dynamics, stress relaxation is found to be promoted primarily by the motion of the particles within the cages formed by the surrounding particles, rather than by cage escape. The stress-relaxation process is accelerated by the permeability of spongy particles, namely due to the sustained volume change that was induced during pre-shear, which renders their cages less effective.

* m.e.a.zakhari@tue.nl

† m.huetter@tue.nl

‡ p.d.anderson@tue.nl

I. INTRODUCTION

A wide variety of applications, where tailored overall properties is an essential requirement, exploits the properties of soft open-porous particles. Among those applications, we mention pharmaceuticals and cosmetics [1, 2], foods [3], and paints [4]. The overall properties of suspensions of these particles emerge from the characteristic properties of the individual particles. These particles combine the elasticity of the supporting porous-network with the viscosity of the permeating fluid, which in turn makes these particles viscoelastic. In practice, these particles can be broadly classified into microgels and star polymers. The elasticity and the permeability of these particles are the reason they are sometimes referred to as poroelastic or permeable particles, and they are often envisaged as sponges, referring to their internal structure. The term *spongy* refers to their ability to deform in both shape and size. In this paper, we refer to these particles as permeable particles. The overall properties of suspensions of permeable particles are tailored through variations of the elastic properties of the particle and their internal structure [5, 6]. The elasticity of the particle allows it to impinge in response to steric effects [7, 8] or applied deformation [9–13], which gives rise to its *elastic softness*. The internal structure of the particle, i.e. the permeability, gives the particle the ability to undergo volume changes, in a rate-dependent manner; this results in its *rate-dependent softness*. It is pointed out that the particles of interest to this work are thus different from hard particles, which are extensively studied theoretically [14], experimentally [15–17], using simulations [18, 19]. In this paper, the particles have both finite elasticity and finite permeability.

Particle systems generally undergo a transition from a liquid-like to a solid-like behavior as system density increases [20]. Concentrated suspensions have been found to undergo slow dynamics [7, 21, 22] and their properties vary in time. The microstructure, during this solidification process, is not fully equilibrated and part of the stress introduced during preparation persists in the system. The non-zero trapped stresses are known as the *residual* or *internal* stress [22–24]. The relaxation of the internal stresses, as the microstructure strives to reach equilibrium, has been found to appreciably affect the rheological properties of the suspension [22, 25]. In permeable-particle suspensions, the competition of the size and position dynamics governs the evolution of the microstructure, which consequently plays an essential role in the stress-relaxation process. It is noteworthy that the size and

position dynamics are related to terms that are common in scattering experiments; namely the structure factor gives information about the particle positions while the form factor is related to the particle sizes and shapes [26].

The phenomenon associated with the slow dynamics of a material as it strives to approach its thermodynamic equilibrium is called aging [27]. It is manifested as the continuous evolution of the thermo-mechanical properties. Aging, in general, also occurs in the absence of load. For instance, the evolution of the properties of dense permeable particle systems is studied in [7] as they are brought from a high-energy state to a long-lived glassy state under no applied deformation. In the case of prior deformation, the residual or internal stresses are the stresses remaining in a material after load removal and that relax slowly as time evolves, being a signal of an ongoing aging process. The stress relaxation upon flow cessation is in fact the focus of this work.

Several efforts have been dedicated to identifying the connection between stress relaxation and the underlying structural changes, in other words, the relative particle arrangement. For instance, in a rheometer, a pre-shear step is performed by applying shear to a suspension for a certain period of time until steady state is reached. Upon cessation of flow at $t = 0$, the shear-stress is measured over time. After the flow is stopped, the stress decays rapidly to a non-zero internal stress value. The subsequent relaxation of the internal stress over time is governed by structural changes. Previous work has been devoted to understanding how the stress-relaxation time (in applied strain measurements) or the strain-relaxation time (in applied stress measurements) τ depends on the time elapsed after flow-cessation, t_{w}. In some of these experiments, a stress (strain) smaller than the yield stress (strain) is applied after a waiting time t_{w} from flow cessation to probe the mechanical properties of the suspension. It is found that the relaxation time depends on t_{w}, that is $\tau(t_{\mathrm{w}})$. In many cases, this dependency has been identified as a power-law $\tau \sim t_{\mathrm{w}}^{\mu}$ as will be described in the following.

Experimental work, on the one hand, gives insight about the effect of the particle softness on the stress relaxation of spongy-particle suspensions. The particle softness, as perceived in experiments, is the combined effect of particle elasticity and the particle permeability, where the former is an elastic softness in nature and the latter is a rate-dependent softness. Purnomo et al. [25] studied the effect of the particle softness of PNIPAM particles on the stress-relaxation behavior. They find that lower particle volume-fraction, and higher particle

softness make the arrest in the glassy state incomplete. Consequently, the stress-relaxation process continues for longer time scales compared to systems with higher volume fraction, and systems with particles of lower softness. They find that, independent of the degree of particle softness, the relaxation time increases linearly with the waiting time, $\mu = 1$ [25]. This is confirmed using particle tracking techniques where this linear dependency is again observed [28]. In contrast, Cloitre et al. [22] show that the relaxation time of polyelectrolyte microgels depends sublinearly on the waiting time, $\mu < 1$, by performing creep experiments. The dependence of the relaxation time on the sample age has been found to depend on the interaction potential. Although it is not necessarily considered spongy, a Laponite suspension forms an example of a system where changes in the interaction potential affect the relaxation process. Increasing salt concentration in Laponite suspensions leads to a less-homogeneous suspension and, consequently, decreases the exponent μ [29]. This already shows that the stress-relaxation behavior is non-universal and rather depends on the specific system studied [30], see also [31] for a detailed review. It is to be noted that the particle softness, in the above-mentioned experimental work, is varied by changing the particle-size [28], cross-link density [23], and the temperature [24, 25]. Adjusting these parameters, however, affects both the particle-permeability as well as the elastic modulus [32, 33]. In contrast, studying the particle-permeability and the elastic modulus independently is experimentally challenging, if at all possible. An example that highlights the importance of the internal degrees of freedom of a different type of soft particles is the work of Erwin et al. [30]. They studied in detail the stress-relaxation process of suspensions of star polymers. They find that the arm relaxation, which can be envisaged as the particle-size change in an effective manner, leads to an accelerated stress relaxation process of star polymers in a terminal regime that follows the two-step relaxation process mentioned before.

Numerical techniques, on the other hand, provide the versatility required in order to vary, independently, the particle permeability and elastic properties. Cloitre, Bonnecaze, and coworkers have used the three-dimensional micromechanical model for soft particles developed in [34] to study the microscopic origin of the stress relaxation in dense soft-particle suspensions [23, 35]. They find that jammed soft-particle suspensions relax through the two-step relaxation mechanism described earlier. The fast relaxation process to a non-zero internal stress immediately after cessation of flow is found to depend on the solvent viscosity, the particle elastic properties, and the volume fraction. The much-slower relaxation

of the internal stress is found to be independent of the material properties. The two-step relaxation was also observed earlier in the work by Gleim et al. [36] using molecular dynamics simulations of particles interacting with a Lennard-Jones potential. Ballauff and coworkers find that the stress relaxation of soft colloidal glasses such as PNIPAM follows a two-decay process, using molecular dynamics simulations and mode-coupling theory [24]. They relate the second decay to the sub-diffusive motion of the particles at long times. Although the above-mentioned numerical efforts provide a link between the particle motion and the corresponding relaxation behavior, the rate-dependent softness that follows from the internal structure of the particle was not considered. The internal structure of the particle is only considered in an effective manner through the particle elastic-modulus. The softness of the particles is achieved through a soft repulsive potential, for instance the Hertzian potential in [23, 35], the Yukawa potential in [24], and the Lennard-Jones potential in [36]. In that sense, treating soft deformable particles as solely elastic oversees the important viscoelastic nature of such particles by not accounting for the particle-size dynamics, in terms of the particle permeability. The particle size- and shape-dynamics can explain why the simulation results of Mohan et al. [23], while considering only the elastic nature of the particle, show a poor agreement with experiments at high pre-shear deformation. Although Mohan et al. consider lubrication effects, which we ignore in the present work, we speculate that not accounting for the viscoelastic nature of the particle can provide a possible explanation for this discrepancy, since these effects are significant at high shear rates, e.g. for size effects, see[9]. An alternative way of accounting for the particle permeability has been described by Nägele and co-workers. They developed a continuum model for the overall behavior of suspensions consisting of solvent and permeable particles. The model describes the evolution of the particle volume fraction in terms of a concentration-dependent collective diffusion coefficient that is also permeability-dependent [37]. Although this model provides an effective way for accounting for the particle permeability, it does not allow for studying the essential features of the material behavior at the scale of the individual particle.

In this paper, we study the stress-relaxation behavior of jammed spongy-particle suspensions taking into account the poroelastic nature of such particles. The internal structure of each particle, i.e. the permeability, is taken into account by considering the particle size as an independent degree of freedom in the model, in addition to the particle position. The particle size-change depends on the permeability of the particle, its elastic properties, and

the viscosity of the permeating solvent. To this end, the dynamic two-scale model developed by Hütter et al. [38] is used. The microscopic level of description provided by the model [38] makes it possible to vary the particle modulus and the permeability independently.

This paper is organized as follows. A brief summary of the model is described in Sec. II followed by a description of the model parameters and the simulation protocol used to obtain the results in Sec. III. The characteristic features of the stress relaxation is given in Sec. IV in view of a comparison between permeable- and impermeable-particle systems. The corresponding particle dynamics during stress relaxation is discussed in Sec. V in terms of the evolution of the mean-square displacement and the particle volume-fraction. In Sec. V, we also link the macroscopic stress-relaxation behavior to the microscopic dynamics. Finally, the paper is concluded with a discussion in Sec. VI.

II. EXTENDED BROWNIAN DYNAMICS MODEL

This section presents, in brief, a realization of the two-scale model developed by Hütter et al. [38]. For more detail, the reader is referred to [9, 38].

Consider a representative volume element at a macroscopic position $\boldsymbol{r}$ that consists of N spherical particles suspended in a Newtonian fluid with a shear viscosity of η. Each particle is described by the position of its center measured relative to $\boldsymbol{r}$, $\boldsymbol{Q}_i$, and its radius R_i. It is to be noted that the particle shape is not taken into account explicitly, but a particle is described by a single scalar quantity, its radius. This means that the model only admits particles that are spherical in shape, see Fig. 1. A $4N$-dimension variable $\boldsymbol{\xi}$ denoting all microscopic degrees of freedom is defined as

$$\boldsymbol{\xi} = \{\boldsymbol{Q}_1, R_1, ..., \boldsymbol{Q}_N, R_N\}. \tag{1}$$

The model describes the evolution of these degrees of freedom over time as they are driven by the (i) a macroscopic velocity field $\boldsymbol{v}$, and (ii) driving forces due to the particle interactions.

In this paper, we impose simple shear, with shear rate $\dot{\gamma}$, flow direction x and gradient direction y,

$$\boldsymbol{v} = \dot{\gamma} y \boldsymbol{e}_x, \tag{2}$$

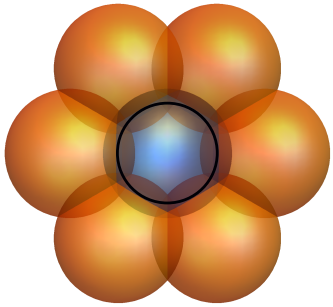

FIG. 1. Schematic representation of the approximation of the particle shape deformation by a radius change, denoted by the black line.

where $\boldsymbol{e}_x$ is the unit vector in the x-direction. The driving forces resulting from the interaction between particles are described as follows. The specific realization of the model is achieved by making a choice of the particle-interaction potential. Particles are assumed to interact through a purely repulsive potential as dense-particle systems are often stabilized and attractive forces are negligible [20, 39, 40]. In the dilute limit, a particle undergoes an elastic volume-change towards its equilibrium size denoted by R_{eq}, driven by the stored elastic energy Φ_i^{vol} [41]. At high densities, a particle impinges with neighboring particles and undergoes an elastic shape-change upon contact, which is described by the Hertzian potential Φ_{ij}^{Hz} [42]. The particle interaction potential is the additive contribution of both the Hertzian and the volumetric energies,

$$\Phi(\boldsymbol{\xi}) = \sum_i \Phi_i^{\text{vol}}(\boldsymbol{\xi}) + \sum_{i \neq j} \Phi_{ij}^{\text{Hz}}(\boldsymbol{\xi}) = E R_{\text{eq}}^3 \tilde{\Phi}(\boldsymbol{\xi}), \tag{3}$$

where E is the Young's modulus and symbol $\tilde{(\cdot)}$ denotes the dimensionless $(\cdot)$. All particles have the same equilibrium size R_{eq}. The dimensionless Hertzian interaction potential between particle i in contact with its neighbor j is

$$\tilde{\Phi}_{ij}^{\text{Hz}}(\boldsymbol{\xi}) = \begin{cases} \frac{1}{2(1-\nu^2)} \left(C\ \tilde{h}_{ij}^m \tilde{R}_c^{3-m} + \tilde{k} \right) & \text{if } \tilde{h}_{ij} > 0, \\ 0 & \text{otherwise,} \end{cases} \tag{4}$$

where ν is the Poisson's ratio and $\tilde{R}_c = \left(\tilde{R}_i^{-1} + \tilde{R}_j^{-1} \right)^{-1}$ is the contact radius, where $\tilde{R}_i$ and $\tilde{R}_j$ are the current particle radii of particles i and j, respectively. All length scales in Eq. (4) and in the remainder of this paper are scaled with R_{eq}. Depending on the degree of overlap

between particles, $\tilde{h}_{ij} = \tilde{R}_i + \tilde{R}_j - |\tilde{\boldsymbol{Q}}_i - \tilde{\boldsymbol{Q}}_j|$, the dimensionless constants $\{C, m, \tilde{k}\}$ in Eq. (4) are defined as

$$\begin{aligned}
\frac{\tilde{h}_{ij}}{\tilde{R}_i + \tilde{R}_j} < 0.1: &\qquad C = \tfrac{8}{15}, \qquad m = \frac{5}{2}, \quad \tilde{k} = 0, \\
0.1 \leq \frac{\tilde{h}_{ij}}{\tilde{R}_i + \tilde{R}_j} < 0.2: &\qquad C = \tfrac{5}{6}\sqrt{\tfrac{5}{2}}, \quad m = 4, \quad \tilde{k} = \frac{\sqrt{10}}{1250}, \\
0.2 \leq \frac{\tilde{h}_{ij}}{\tilde{R}_i + \tilde{R}_j} < 0.6: &\qquad C = \tfrac{125}{144}\sqrt{\tfrac{5}{2}}, m = 6, \quad \tilde{k} = \frac{89\sqrt{10}}{11250},
\end{aligned} \tag{5}$$

which ensure the continuity of energy and force. The reader is referred to Appendix A of [7] for more details. The dimensionless volumetric energy is defined as [41]

$$\tilde{\Phi}_i^{\mathrm{vol}} = \frac{2\pi}{9(1-2\nu)} \left(\tilde{R}_i^3 - 1\right)^2, \tag{6}$$

where $\tilde{R}_i^3 - 1$ is the volumetric strain compared to the equilibrium size.

The evolution of the particle position and size is expressed in the form of stochastic differential equations [38]. These equations are applied in this work in terms of the dimensionless potential energy Eq. (3) and the imposed flow field Eq. (2). In this work, the single-particle Stokes' drag is the only form of hydrodynamic interaction with the background solvent acting on the particle positions, which is captured via the friction coefficient $\zeta_{Q_i} = 6\pi\eta R_i$. The reasons for neglecting the many-particle hydrodynamic interactions are the following: (i) Since the main goal of this paper is to conduct an extensive study of the particle permeability and the particle elasticity, the computational cost involved in also accounting for many-particle hydrodynamic interactions in both shear and flow cessation would significantly hamper achieving this goal. (ii) The particles of interest to the present work form a model system for two broad types of particles, namely star polymers and microgels [20]. These particles have surface features that make their thermodynamic radius, R^{th}, larger than their hydrodynamic radius, R^{h}. Many-particle hydrodynamic interactions are dominant when these radii are of the same order. According to Brady and coworkers, the viscosity of the solvent can be considered unaffected by the flow around the particles for $\left(R^{\mathrm{th}} - R^{\mathrm{h}}\right)/R^{\mathrm{h}} \gtrapprox 2$ [43, 44]. This ratio is rather common for the particles of interest, see for instance, the size of the core, R^{h}, vs. the thickness of the shell, $R^{\mathrm{th}} - R^{\mathrm{h}}$, in the core-shell particles in [45, 46]. Furthermore, Nägele and coworkers argue that the hydrodynamic radius of the particle decreases with increasing the particle permeability since more solvent is allowed to penetrate the particle [37]. In addition, it is assumed that the irreversible particle

position (size) changes are driven solely by the derivative of the potential energy with respect to the particle position (size), i.e. neglecting dynamic cross-coupling between position and size (see [38] for more details). The size-dynamics of different particles are assumed to be hydrodynamically uncoupled. The position- and size-dynamics in dimensionless form are, respectively, (see [7] for more detail),

$$d\tilde{\boldsymbol{Q}}_i = \mathrm{Pe}\,\tilde{Q}_{i,y}\boldsymbol{e}_x d\tilde{t} + \frac{1}{S^*}\left(-\boldsymbol{\nabla}_{\tilde{\boldsymbol{Q}}_i}\tilde{\Phi}\right)d\tilde{t} + \sqrt{2}\ \left[d\tilde{\boldsymbol{W}}_t\right]_{\boldsymbol{Q}_i}, \tag{7a}$$

$$d\tilde{R}_i = \frac{\zeta^*}{S^*}\left(-\partial_{\tilde{R}_i}\tilde{\Phi}\right)d\tilde{t} + \zeta^*\left(\partial_{\tilde{R}_i}\ln\zeta_{R_i}^{-1}\right)d\tilde{t} + \sqrt{2\zeta^*}\ \left[d\tilde{W}_t\right]_{R_i}, \tag{7b}$$

where $\tilde{Q}_{y_i}$ denotes the y-component of $\tilde{\boldsymbol{Q}}_i$. The time in Eq. (7) is scaled with the Brownian time scale $\tau_Q^{\mathrm{Br}} = 6\pi\eta R_{\mathrm{eq}}^3/k_{\mathrm{B}}T$, i.e.

$$\tilde{t} = t/\tau_Q^{\mathrm{Br}}. \tag{8}$$

The Brownian time scale is the time at which a particle diffuses its radius due to thermal fluctuations. The driving forces for position-change and size-change are, $-\boldsymbol{\nabla}_{\tilde{Q}_i}\tilde{\Phi}$ and $-\partial_{\tilde{R}_i}\tilde{\Phi}$, respectively. In the general case, the particle-size dynamics (7b) is driven by $\tilde{F}_R = \tilde{F}_R^{\mathrm{Hz}} + \tilde{F}_R^{\mathrm{vol}}$, where $\tilde{F}_R^{\mathrm{Hz}} = -\partial_R\tilde{\Phi}^{\mathrm{Hz}}$ and $\tilde{F}_R^{\mathrm{vol}} = -\partial_R\tilde{\Phi}^{\mathrm{vol}}$. In the dilute limit, i.e. $\tilde{\Phi}^{\mathrm{Hz}} = 0$, the particle-size dynamics (7b) is driven by $\tilde{F}_R = \tilde{F}_R^{\mathrm{vol}}$ and the size dynamics is decoupled from the position. It is pointed out that, osmotic effects can be included effectively by appropriate choices of the material parameters in $\tilde{\Phi}^{\mathrm{Hz}}$ and $\tilde{\Phi}^{\mathrm{vol}}$. The fluctuating Brownian contributions are given by the terms involving the Wiener-process increments $[d\tilde{\boldsymbol{W}}_t]_{\boldsymbol{Q}_i}$ and $[d\tilde{W}_t]_{R_i}$, in the position and size equations, respectively. The Wiener-process increment, akin to Brownian fluctuations, has the following properties: (i) an average of $\langle d\tilde{\boldsymbol{W}}_t\rangle = 0$ and (ii) a variance of $\langle d\tilde{\boldsymbol{W}}_t d\tilde{\boldsymbol{W}}_{t'}\rangle = \delta_{t,t'}d\tilde{t}\boldsymbol{I}$, where $\boldsymbol{I}$ is the identity tensor. The size mobility is $\zeta_{R_i}^{-1} = R_{\mathrm{eq}}^3\chi/\left(12\pi\eta R_i^4\right)$, where χ is a dimensionless permeability measure. Based on the theory of poroelasticity [47], χ is given by $\chi = \pi^2\kappa/R_0^2$, with κ being the permeability and R_0 being the initial particle size, that is the particle size prior to shearing, which is specified in Sec. III.

Equation (7) is expressed in terms of three dimensionless groups that fully describe the system studied, these are $(S^*, \zeta^*, \mathrm{Pe})$. The first dimensionless number, S^*, is a measure of the particle elastic softness expressed in units of the thermal energy $k_{\mathrm{B}}T$. The Péclet number, Pe, compares the shear time to the time a particle requires to diffuse its own size due to thermal noise [48]. The dimensionless group that characterizes the particle internal structure, that is the permeability, is denoted by ζ^*. These dimensionless groups are defined

as

$$S^* = \frac{k_\mathrm{B}T}{ER_\mathrm{eq}^3}, \tag{9a}$$

$$\mathrm{Pe} = \dot{\gamma}\tau_Q^\mathrm{Br}, \tag{9b}$$

$$\zeta^* = \frac{\chi}{2}. \tag{9c}$$

It is to be noted that S^*, as defined by Eq. (9a) is the inverse of the elasticity parameter defined by Vlassopoulos and coworkers, see e.g. [20], which is of order unity for polymer coils, so as S^*. To obtain S^* of order unity for other (harder) particles, one could express S^* in terms of elastic energy for volume change, that is approximately equal to $k_\mathrm{B}T/(4\pi ER_\mathrm{eq}^2\Delta R)$, where ΔR is the typical magnitude of the radius change. However, the definition of S^* given by Eq. (9a) is convenient for scaling the evolution equations (7).

Based on the quantities defined just above, several characteristic time scales can be deduced, for the purpose of physical interpretation. For example, the interaction energy is dissipated through viscous damping over time scales $\tau_Q = S^*\tau_Q^\mathrm{Br}$ and $\tau_R = (S^*/\zeta^*)\,\tau_Q^\mathrm{Br}$, for position-change and size-change, respectively. In addition, the characteristic time scale for size-relaxation is given by $\tau_R^\mathrm{Br} = \tau_Q^\mathrm{Br}/\zeta^*$. Finally, the characteristic shear time is given by $\tau_\gamma = \tau_Q^\mathrm{Br}/\,\mathrm{Pe}$.

Changes at the microscopic level, i.e. in particle size and position, described by Eq. (7) lead to stresses on the macroscopic level. These stresses are used to describe the effective overall behavior of suspensions of spongy-particles. The constitutive relation governing the behavior of spongy-particle systems is derived in [38]. In this work, the shear stress component σ_{xy} is studied, in compliance with the applied deformation (2). The shear stress contains only a contribution originating from the interaction forces between particles due to their relative position with respect to other neighboring particles. The particle size change, on the other hand, leads to only isotropic contributions. The dimensionless stress tensor due to the particle interaction, scaling all length scales by R_eq and using the dimensionless interaction potential, is

$$\tilde{\sigma}_{xy} = \frac{\sigma_{xy}}{E} = nR_\mathrm{eq}^3\left\langle \sum_i (\nabla_{\tilde{\boldsymbol{Q}}_i}\tilde{\Phi})\tilde{\boldsymbol{Q}}_i \right\rangle. \tag{10}$$

The reader is referred to [38] for the full derivation of the stress tensor. The Newtonian solvent contribution to the stress is not described in our model, but it could be included in

a straightforward way [49]. In the dilute limit, where particles do not overlap, i.e. $\tilde{\Phi}^{\mathrm{Hz}} = 0$, only an isotropic contribution to the stress pertains due to size deviations from the equilibrium size. In this case, $\tilde{\sigma}_{xy} = 0$ upon flow cessation.

III. NUMERICAL SIMULATIONS, PARAMETER SPECIFICATION

The systems modeled consist of 1728 particles suspended in water with a shear viscosity η. Particles are initially placed on a simple cubic lattice in a cubic box and their initial size R_0 is equal to the equilibrium size R_{eq}. The volume of the simulation box is kept constant over the simulation time. The simulation box is subjected to Lees-Edwards periodic boundary conditions [50]. Equation (7) is solved numerically using a forward-Euler integration scheme [51]. The time step used for the integration scheme, $\Delta\tilde{t}$, is set to 4.81×10^{-5}, which is small enough to capture the fast dynamics. The shortest time scale in all our simulation is found to be $\tau_Q = S^* \tau_Q^{\mathrm{Br}}$. The time step is set to be two orders of magnitude smaller than $\tilde{\tau}_Q$, i.e. $\Delta\tilde{t} \leq 10^{-2}\tilde{\tau}_Q$. In order to highlight the effect of the particle-size changes and since particle-size changes due to steric effects are found to be more significant at volume fractions higher than 0.8 as observed in experiments [8] and simulations [7], a dense system of permeable particles with a number density of $n = 1.3 \times 10^{19}$ m^{-3} is studied. This number density corresponds to a volume fraction,

$$\varphi_{\mathrm{free}} = \frac{4}{3}\pi R_{\mathrm{eq}}^3 n, \tag{11}$$

based on the equilibrium size R_{eq}, of $\varphi_{\mathrm{free}} = 0.850$. At this density, the suspension is considered jammed. This system is used to demonstrate the characteristic features of the stress evolution over time.

The physical values of the model parameters used throughout this paper is given in Table I, while Table II gives parameters used in the actual numerical simulations based on the physical parameters given in Table I. We have shown in [7] that for dense systems increasing the system size has a moderate effect only on the long-time behavior. One can always improve the accuracy of the results by increasing the system size at the expense of the computational cost. However, since the aim of this paper is to compare the relaxation behavior of permeable- vs. impermeable-particle systems, we compare these systems at the same system size and under the same conditions. The particles modeled in this work are

permeable particles that have similar properties to materials used in biomimetic application, for instance, polyacrylamide gels used as substrates for neural cell growth [52], $S^* \sim 10^{-3}$. Moreover, in order to show the effect of the particle-size change, particles with higher softness, $S^* \sim 10^{-2}$, are also modeled. The Brownian time, used to scale all involved time scales, is $\tau_Q^{\mathrm{Br}} = 7.28 \times 10^{-2}$ s.

TABLE I. Physical parameters.

Parameter	Symbol	Physical value
Equilibrium particle radius	R_{eq}	2.5×10^{-7} m
Solvent shear viscosity	η	10^{-3} Pa s
Poisson's ratio	ν	0.4
Young's modulus	E	$\{3, 10, 30, 100\}$ Pa
Permeability	κ	$6.3 \times \{0, 10^{-16}\}$ m^2
Temperature	T	293 K

TABLE II. Model parameters.

Parameter	Symbol	Physical value
Number of particles	N	12^3
Volume fraction	φ_{free} (based on Eq. (11))	0.850
Softness, dimensionless	S^*	$\{86, 26, 8.6, 2.6\} \times 10^{-3}$
Permeability, dimensionless	ζ^*	$\{0, 5\} \times 10^{-2}$
Péclet number	Pe	Pe ≥ 0.5

The numerical experiments performed follow the protocol shown in Fig. 2. The protocol followed in this paper mimics the experimental protocol of [53] in which strain-controlled

experiments are performed and the stress is monitored over time immediately after load removal, i.e. for waiting time $t_{\mathrm{w}} = 0$. The main difference is that the simulations are performed at constant system volume while in experiments a constant pressure approach is preferred. It is to be noted that a similar protocol to what is used in the present paper has been used to obtain the simulation results in [23]. The many-particle system is subject to simple shear deformation with a pre-shear value of $\dot{\gamma}_{\mathrm{p}}$ for a period of approximately $385\tau_Q^{\mathrm{Br}}$. It is to be noted that this pre-shear simulation time is long enough to see no change in the reached state and hence the latter can be considered a steady state. The pre-shear is switched off at $\tilde{t} = 0$ and the evolution of the shear stress of this jammed system is observed over time for a period of $10\tau_Q^{\mathrm{Br}}$. In that sense, the time as expressed by $\tilde{t}$ is measured relative to the time at the end of the pre-shear step. The Péclet numbers calculated are based on $\dot{\gamma}_{\mathrm{p}}$. Every simulation is performed with five different realizations of the noise. The data presented in the following sections are based on the average of these five simulations. It is to be noted that these systems at high Pe undergo a transition to an ordered state [9]. However, in this paper we present the stress relaxation of systems that do not undergo this transition within the simulation time for pre-shear, i.e. $385\tau_Q^{\mathrm{Br}}$. So doing, we eliminate the effect of the different structures that develop during pre-shear, such as the tilted string phase and the straight string phase. The reader is referred to [9] for more details.

IV. STRESS RELAXATION

In this section, we discuss the stress relaxation after shear-flow cessation for different pre-shear conditions. The stress-relaxation behavior is described in view of a comparison between a permeable-particle system $\zeta^* = 0.05$ and an impermeable-particle system $\zeta^* = 0$, where both systems have the same elastic softness $S^* = 2.6\times10^{-3}$, unless otherwise specified. The stress-relaxation behavior is described in the following in terms of two quantities: (i) the (internal) stress values and (ii) the characteristic relaxation time.

First, we discuss the behavior observed in Fig. 3 in terms of the stress values. Figure 3 shows the shear-stress decay as a function of time after flow cessation for a permeable- and an impermeable-particle system at different pre-shear conditions. As the Péclet number increases, the pre-shear stress increases which can be seen from the initial part of the curves shown in Fig. 3 (approximately up to $\tilde{t} = 10^{-3}$). The shear stress decays rapidly to a finite

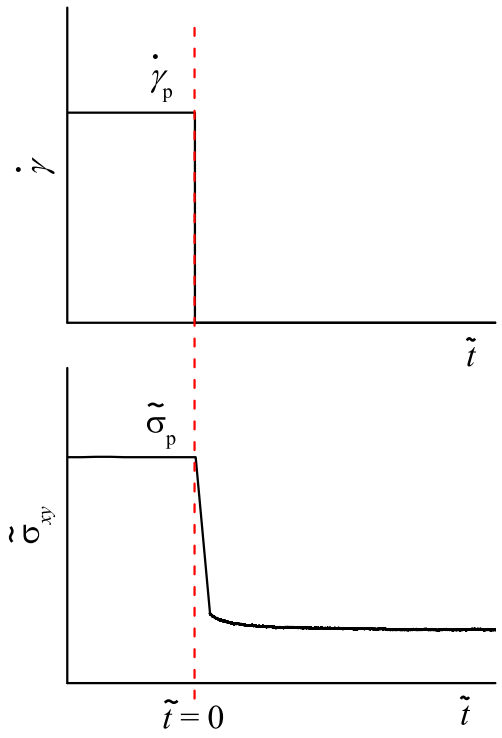

FIG. 2. Simulation protocol. The upper panel shows the applied shear rate over time, and the lower panel shows the corresponding shear stress over time. The red dashed line marks the start of the flow-cessation experiment.

value of stress, which we denote by $\tilde{\sigma}_\mathrm{i}$. The relaxation of the internal-stress $\tilde{\sigma}_\mathrm{i}$ proceeds at much slower rates. The internal stress is obtained from fitting the data on a linear time scale to an exponential decay where the internal stress is the stress at long times. We find that the internal stress decreases with increasing Pe for both systems. The internal stress $\tilde{\sigma}_\mathrm{i} < 0.01\tilde{\sigma}_\mathrm{p}$ for both systems at $\mathrm{Pe} = 3.64$. For this reason, the internal stress for permeable- and impermeable-particle systems shown in Fig. 3 in red lines is only shown for $\mathrm{Pe} = 0.73$ where the internal stress is largest. The decrease of the internal stress with increasing Péclet number is observed in the experimental results of Ballauff et al. [24] for PNIPAM and in line with the numerical results of Mohan et al. [23] of elastic particles. Comparing the internal stress for permeable and impermeable particles, we find that the internal stress of permeable particles is higher than that of impermeable particles at a given Pe. This can be explained by considering their corresponding pre-shear stresses. At a given pre-shear, the shear-stress response is higher for impermeable-particle system than permeable-particle system [9]. Mohan et al. has found that the smaller the pre-shear stress the larger are the

internal stresses for a given system [23].

Second, the characteristic relaxation-time of the stress is studied in the following. In this work, we follow the approach of extracting one overall time-scale that is characteristic of the relaxation process, instead of identifying the different modes in the two-step stress relaxation as explaind in Sec. I. This procedure facilitates the comparison between (i) permeable- and impermeable-particle systems, and (ii) different microscopic time scales. Consider the sample stress curve given in Fig. 4. To determine the characteristic relaxation-time, the stress-relaxation curve is shifted vertically with the internal stress, leading to $\tilde{\sigma}_{xy}(\tilde{t}) - \tilde{\sigma}_{\rm i}$. In order to eliminate the effect of the pre-shear stress, this curve is then normalized by its initial value, which is $\tilde{\sigma}_{\rm p} - \tilde{\sigma}_{\rm i}$. This procedure gives a function $f_\sigma(\tilde{t}) = (\tilde{\sigma}_{xy}(\tilde{t}) - \tilde{\sigma}_{\rm i})/(\tilde{\sigma}_{\rm p} - \tilde{\sigma}_{\rm i})$, that starts at unity and decays to zero. The integral of $f_\sigma(\tilde{t})$ over time increases up to a plateau value, which is used as the measure for the characteristic relaxation-time. We have noticed that the integral values sustain large fluctuations if the time integration is extended far into the stress plateau, due to significant stress fluctuations in the steady state. To obtain a good estimate of the relaxation time, we use the following procedure. Fitting $\sigma_{xy}(\tilde{t})$ with an exponential function to determine $\tilde{\sigma}_{\rm i}$, one also obtains the corresponding decay time $\tau_{\rm fit}$. Since the stress relaxation may not be truly exponential, $\tau_{\rm fit}$ is not necessarily a good measure for the relaxation time of the stress. Rather, the integral $I_s = \int_0^s f_\sigma(\tilde{t})dt$ gives the actual stress relaxation time, if the value for s is appropriately chosen. In our case, we choose $\tilde{\tau}_\sigma = \langle I_s \rangle_{s\in[3\tau_{\rm fit}, 4\tau_{\rm fit}]}$, which is the average of I_s over the s-interval $[3\tau_{\rm fit}, 4\tau_{\rm fit}]$. This range was chosen because in this range the stress is smaller than 5% of its initial value. The relaxation time of the shear stress as a function of pre-shear Pe is given in Fig. 5 for particles with different elastic moduli. The systems corresponding to those shown in Fig. 3 are marked with the dashed lines. Both systems, permeable and impermeable, show a decrease in relaxation time with increasing Pe, which is in accordance with the work of Mohan et al. [23, 35] and Fritschi et al. [54]. However, at a given Pe, permeable particles are found to relax on shorter time scales than impermeable particles of the same elastic modulus, particularly for systems with low S^*. The exception to this trend is observed for the two systems with the highest S^* at Pe = 0.73. In this case, the fluctuations of the long time stress values are large, in particular larger than 20% of the corresponding pre-shear stress, and so the determination of the relaxation time-scale is intrinsically difficult at Pe = 0.73. In general, the difference between the time scales between permeable and impermeable

particles decreases as Pe increases. The accelerated relaxation process of permeable particles is attributed to their additional degree of freedom, that is the size. They can adjust their size to accommodate the forces from the neighboring particles and the applied deformation in the pre-shear stage, which leads to lower volume fraction at the start of the stress-relaxation experiment. It is observed in previous work that, for a certain system, the stress relaxation occurs over shorter time scales at low-volume fraction than at high-volume fraction, see for instance [24, 55]. We show in the following that the relaxation process of permeable particles is not only affected by the particle-position dynamics, but also by the particle-size dynamics which was initially driven away from equilibrium during pre-shear.

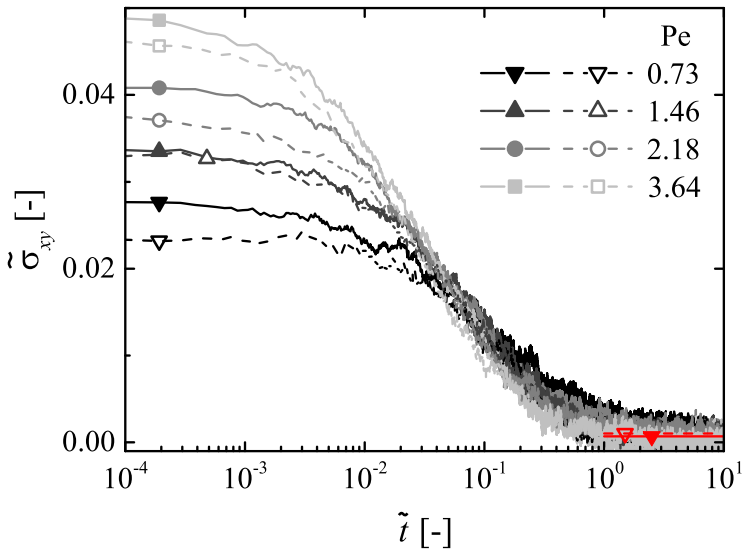

FIG. 3. Shear stress, $\tilde{\sigma}_{xy}$, over time for an impermeable-particle system (solid lines) with $\zeta^* = 0$ and a permeable particle system (dashed lines) with $\zeta^* = 0.05$, and $S^* = 2.6 \times 10^{-3}$ for both systems. The pre-shear stresses $\tilde{\sigma}_{\mathrm{p}}$ corresponding to Pe $= \{0.73, 1.46, 2.18, 3.64\}$ denoted in the figure are $\{2.84, 3.63, 4.21, 5.07\} \times 10^{-2}$ and $\{2.63, 3.37, 3.90, 4.70\} \times 10^{-2}$, for impermeable and permeable particles, respectively. Prior to shearing, the density of these systems is $\varphi_{\mathrm{free}} = 0.850$ ($n = 1.3 \times 10^{19}$ m^{-3}). The red lines show the internal stress values $\tilde{\sigma}_{\mathrm{i}}$ for both permeable and impermeable particles at Pe $= 0.73$.

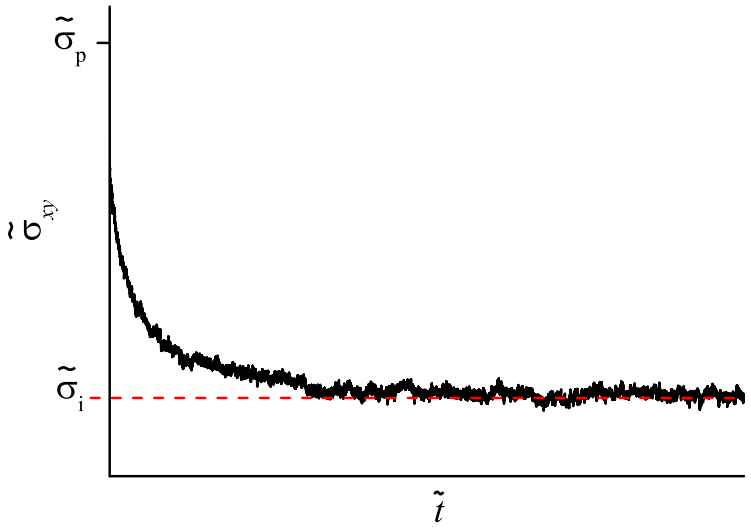

FIG. 4. Schematic representation of shear stress versus time, $\tilde{\sigma}_{xy} - \tilde{t}$, curve. In order to obtain the relaxation time scale, a function $f_\sigma(\tilde{t}) = (\tilde{\sigma}_{xy}(\tilde{t}) - \tilde{\sigma}_\mathrm{i})/(\tilde{\sigma}_\mathrm{p} - \tilde{\sigma}_\mathrm{i})$ is calculated based on the pre-shear, $\tilde{\sigma}_\mathrm{p}$, and internal stress, $\tilde{\sigma}_\mathrm{i}$, values as shown in the plot.

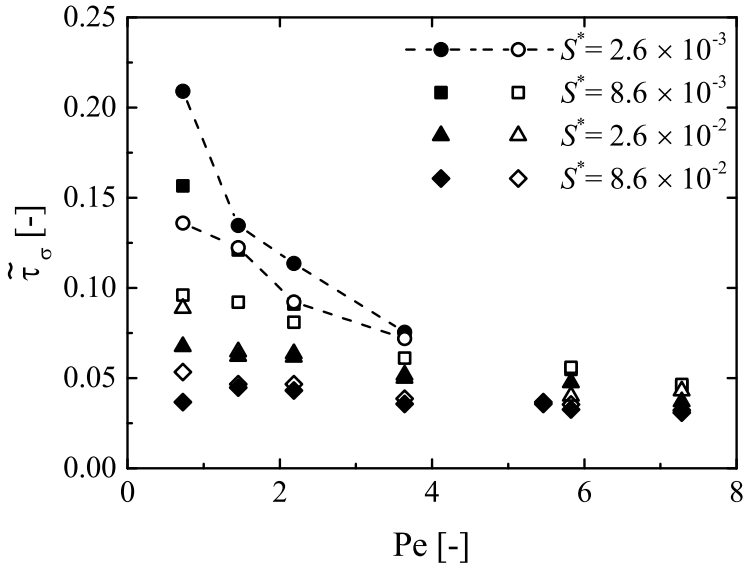

FIG. 5. Relaxation time of the shear stress, $\tilde{\tau}_\sigma$, as a function of Pe for impermeable particles (closed symbols) with $\zeta^* = 0$ and permeable particles (open symbols) with $\zeta^* = 0.05$, at different particle elastic-softness S^*. Prior to shearing, the density of these systems is $\varphi_\mathrm{free} = 0.850$ ($n = 1.3 \times 10^{19}$ m^{-3}). Dashed lines connect data points corresponding to simulations shown in Fig. 3.

V. PARTICLE DYNAMICS DURING STRESS RELAXATION

The particle dynamics during stress-relaxation is studied in this section. The particle-dynamics is described in terms of the mean-square displacement (MSD) of the particles and the actual particle volume-fraction over time. The systems investigated in this section are a permeable-particle system $\zeta^* = 0.05$ and an impermeable-particle system $\zeta^* = 0$, where we vary the particle elastic properties, i.e. S^*.

A. Mean-square displacement

The mean-square displacement is used to characterize the position dynamics of the particles. It is calculated based on the displacement vector of a particle i measured with respect to the time at flow cessation, $\tilde{t} = 0$. The displacement vector is expressed as, $\delta\tilde{\boldsymbol{Q}}_i(\tilde{t}) = \tilde{\boldsymbol{Q}}_i(\tilde{t}) - \tilde{\boldsymbol{Q}}_i(0)$, where $\tilde{\boldsymbol{Q}}$ is $\boldsymbol{Q}$ scaled with R_{eq}. The MSD is calculated as

$$\text{MSD}(\tilde{t}) = \text{tr}\left(\left\langle \delta\tilde{\boldsymbol{Q}}_i(\tilde{t}) \otimes \delta\tilde{\boldsymbol{Q}}_i(\tilde{t}) \right\rangle_N\right), \tag{12}$$

where $\langle\cdot\rangle_N$ is the average over the number of particles N. The evolution of the MSD is measured over the course of the simulation time.

Figure 6 shows the MSD corresponding to the systems shown in Fig. 3. It can be seen in Fig. 6 that systems subjected to higher pre-shear exhibit larger MSD at a given time. Although this behavior is observed for both permeable- and impermeable-particle systems, Fig. 6 shows that, at a certain instant in time, permeable particles diffuse more than impermeable particles subjected to the same pre-shear. This is attributed to the fact that the volume fraction of permeable particles is lower than that of impermeable particles, due to their ability to change in size when subjected to deformation. This is described in detail in the following sections. Focusing on one of the curves in Fig. 6, we see that particles diffuse rapidly after flow-cessation as seen by the slope of the initial part of the curve. The diffusion of the particles is slowed down at intermediate times. The transition between fast and slow diffusion characterizes the increased hindrance of the particle motion by the surrounding particles that form a cage. At even longer times, the particles can escape their cages and their diffusion increases, till they get trapped in the next cage (not shown in Fig. 6)

In the following, we compare the particle diffusion of permeable and impermeable particles in terms of the characteristic features in MSD behavior. The time at which (i) a particle is

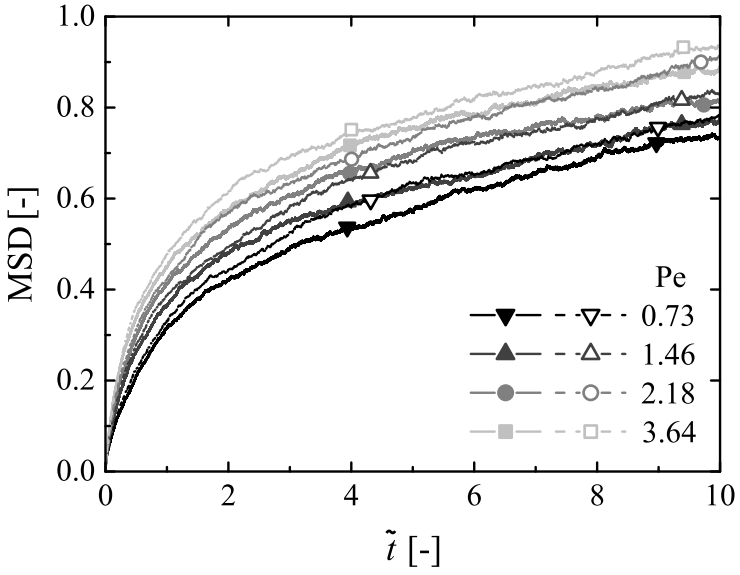

FIG. 6. Mean-square displacement MSD over time for an impermeable-particle system (solid lines) with $\zeta^* = 0$ and a permeable particle system (dashed lines) with $\zeta^* = 0.05$ and $S^* = 2.6 \times 10^{-3}$ for both systems. Prior to shearing, the density of these systems is $\varphi_{\text{free}} = 0.850$ ($n = 1.3 \times 10^{19}$ m^{-3}).

increasingly hindered by neighboring particles and (ii) the time at which a particle escapes the restriction of the neighboring particles, are used as the characteristic MSD times. The former is denoted by $\tilde{\tau}^{\text{cage}}_{\text{MSD}}$, while the latter is denoted by $\tilde{\tau}^{\text{esc}}_{\text{MSD}}$. A *cage* is the confinement of the particle by the neighboring particles, which in turn restricts its mobility until occasional cage escape occurs. The characteristic time $\tilde{\tau}^{\text{cage}}_{\text{MSD}}$ can be seen in the MSD as the time at which the slope of the MSD curve changes to lower values. Figure 7 shows the MSD for the systems shown in Fig. 6 on a log-log scale. It is found that at short times the process is diffusive ($\alpha \approx 1$), then evolves into sub-diffusive ($\alpha < 1$), where α is the slope of the MSD-time curve on a double logarithmic scale. For simulations where cage-escape was observed (not shown in Fig. 7) emergent diffusive behavior was found. This result is in accordance with the behavior found for colloidal glasses, see for instance [31, 56].

In order to obtain $\tilde{\tau}^{\text{cage}}_{\text{MSD}}$, we approximate the behavior of the MSD curve (Fig. 6) by a ninth-order polynomial to capture the main features of the MSD curve. The first minimum of the second derivative of the polynomial is $\tilde{\tau}^{\text{cage}}_{\text{MSD}}$. A clear dependence of $\tilde{\tau}^{\text{cage}}_{\text{MSD}}$ on the pre-shear rate, S^*, or ζ^* is not detected. However, it is found that breaking of the cages occurs at $\tilde{\tau}^{\text{cage}}_{\text{MSD}} \sim 10^{-3} - 10^{-2}$. This result is shown explicitly in Sec. V C, where the different time scales are compared for the purpose of identifying the microscopic origin for

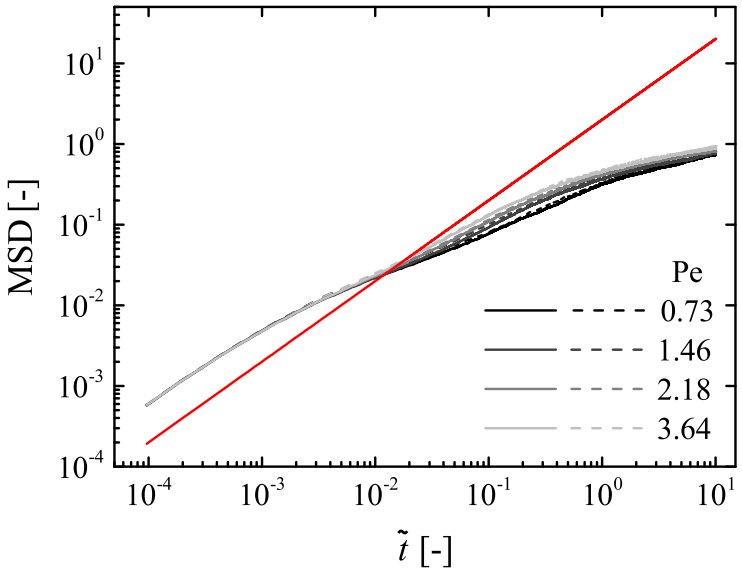

FIG. 7. Double logarithmic plot of the mean-square displacement MSD over time for an impermeable-particle system (solid lines) and a permeable particle system (dashed lines) corresponding to Fig. 6. The red line indicates the mean square displacement for a diffusive process with slope of unity.

stress relaxation. On the other hand, the time at which particles escape their cages, $\tilde{\tau}^{\mathrm{esc}}_{\mathrm{MSD}}$, is used to further characterize the MSD. To obtain this time, we calculate the distance between the particles in a system with the closest packing achievable for these systems. In equilibrium, the most stable structure in this case is the FCC structure [7]. The volume fraction of FCC is $\varphi_{\mathrm{FCC}} = 0.74$. Based on the FCC structure, the average distance between particles is $d = \sqrt[3]{6\varphi_{\mathrm{FCC}}/(\pi n)}$. For the system studied in this work, we obtain $\tilde{d} = 1.9095$. The characteristic MSD time $\tilde{\tau}^{\mathrm{esc}}_{\mathrm{MSD}}$ is defined as the time at which MSD $= \tilde{d}^2$. Figure 8 shows $\tilde{\tau}^{\mathrm{esc}}_{\mathrm{MSD}}$ as a function of Pe for systems with different elastic properties. It is found that permeable particles escape their cages faster than impermeable particles for a given pre-shear. Figure 8 also shows that this time scale increases with increasing the elastic modulus of the particle. These observations will be revisited later in view of the volume fraction of the system. It is noteworthy that $\tilde{\tau}^{\mathrm{esc}}_{\mathrm{MSD}}$ is larger than the simulation time for the systems with $S^* = 2.6 \times 10^{-3}$ (corresponding to Fig. 6) and for the impermeable particles with $S^* = 8.6 \times 10^{-3}$. Hence, the corresponding data are not shown in Fig. 8. In addition, for permeable particles with $S^* = 8.6 \times 10^{-3}$, particles form ordered structures at the end of the shear simulation for pre-shear Pe $\gtrsim 20$ and, so these data are also not shown in Fig. 8.

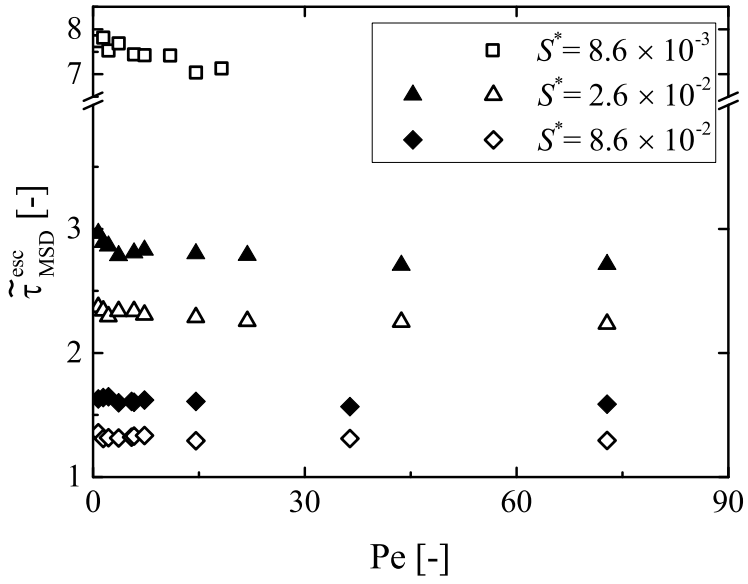

FIG. 8. Relaxation time of the particle MSD, $\tilde{\tau}^{\rm esc}_{\rm MSD}$, as a function of Pe for impermeable particles (closed symbols) with $\zeta^* = 0$ and permeable particles (open symbols) with $\zeta^* = 0.05$, at different particle elastic-softness S^*. Prior to shearing, the density of these systems is $\varphi_{\rm free} = 0.850$ ($n = 1.3 \times 10^{19}$ m^{-3}).

B. Volume fraction

The volume fraction is used to characterize the particle size over time. The volume fraction at a certain time $\tilde{t}$ is calculated based on the sum of the size of all particles at this time compared to the volume of the simulation box,

$$\varphi = \frac{\sum_i^N \frac{4}{3}\pi R_i^3}{N} n. \tag{13}$$

It is to be noted that, for the impermeable-particle system, the volume fraction remains constant over time and equal to the initial volume fraction prior to shearing, $\varphi_{\rm free} = 0.850$, because impermeable particles are not able to change in size.

Figure 9 shows the evolution of the volume fraction over time corresponding to the permeable- and impermeable-particle systems in Fig. 3. This figure shows that the volume fraction of the permeable-particle system is smaller than 0.850. We also find that the deviation from the initial volume fraction is higher for larger pre-shear values at the start of the flow-cessation simulation (at $\tilde{t} = 0$). Permeable particles are driven to low-volume fraction by the applied shear at $\tilde{t} < 0$ [9]. At $\tilde{t} \geq 0$ as the applied shear is stopped, perme-

able particles strive to reach their equilibrium size over time. The equilibrium size denoted by R_{eq} is the size that the particle would attain in the dilute limit. However, the balance of Hertzian and volumetric forces does not allow the particles to reach R_{eq}, but rather a new equilibrium size $R_{\text{eq}}^{\text{new}} < R_{\text{eq}}$ is reached due to constraints. For permeable particles for the systems in Fig. 9, particles relax to $R_{\text{eq}}^{\text{new}}$ corresponding to a volume fraction of approximately 0.838, independent of the pre-shear.

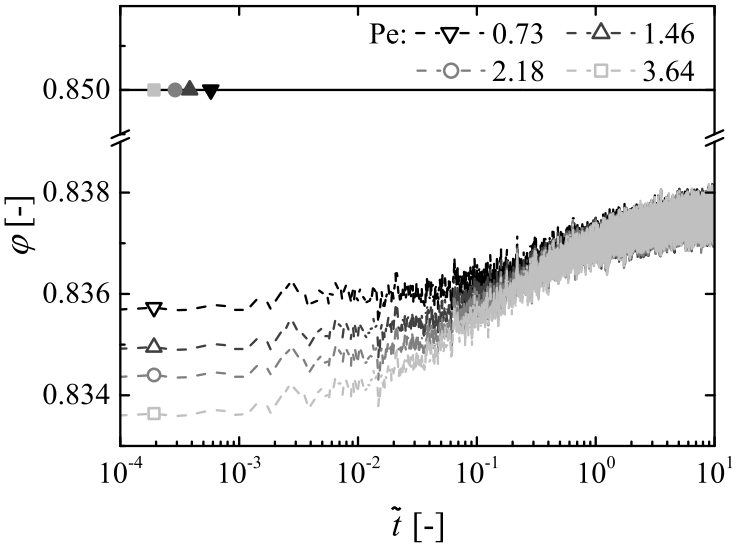

FIG. 9. Particle volume-fraction, φ, over time for an impermeable-particle system (solid line) with $\zeta^* = 0$ and a permeable particle system (dashed lines) with $\zeta^* = 0.05$ and $S^* = 2.6 \times 10^{-3}$ for both systems. Prior to shearing, the density of these systems is $\varphi_{\text{free}} = 0.850$ ($n = 1.3 \times 10^{19}$ m^{-3}).

We study the relaxation of the particle volume-fraction over time in terms of a relaxation time that describes the approach of the volume fraction towards equilibrium. The relaxation time for the volume fraction is obtained using a similar procedure used to obtain $\tilde{\tau}_\sigma$, that is using a function $f_\varphi(\tilde{t}) = (\varphi(\tilde{t}) - \varphi(\tilde{t} \to \infty))/(\varphi(0) - \varphi(\tilde{t} \to \infty))$. The integral of the volume fraction function, $f_\varphi(\tilde{t})$ gives the relaxation time $\tilde{\tau}_\varphi$ (see Section IV for more details). Figure 10 shows the relaxation time for the volume fraction as a function of Pe for permeable particles with different elastic-softness S^*. First of all, it is to be noted that the volume fraction at $\tilde{t} = 0$ is close to the value of the volume fraction at long times (see Fig. 9). Hence, the quality of the integral calculation is lowest at low Pe. We see that the relaxation time for the volume fraction is smaller as the pre-shear is increased (see, for instance, dashed line in Fig. 10). Based on Equation (7b), the relaxation time of the particle size depends, on

the one hand, on the driving force $\partial_{\tilde{R}_i}\tilde{\Phi}$ and, on the other hand, on the transport coefficient ζ^*/S^*. For a system with a given ζ^* and S^*, i.e. at a fixed transport coefficient, particles are driven further away from their equilibrium size as the applied pre-shear increases. The larger difference in size means that the elastic strain energy per particle and the corresponding driving force for size change are higher (see Eq. 6). Consequently, the relaxation of the size towards equilibrium occurs faster at higher Pe. Comparing systems with different S^* at a given Pe, the trend in the behavior of $\tilde{\tau}_\varphi$ is difficult to predict based on Eq. (7), because the particle softness enters in both the position and size dynamics, respectively, these equations are mutually coupled. The numerical simulations reveal the following behavior. We see in Fig. 10 that the overall volume fraction of elastically softer particles, i.e. particles with larger S^*, relaxes faster than for elastically harder particles (see for instance $\tilde{\tau}_\varphi$ at Pe = 3.64 in Fig. 10).

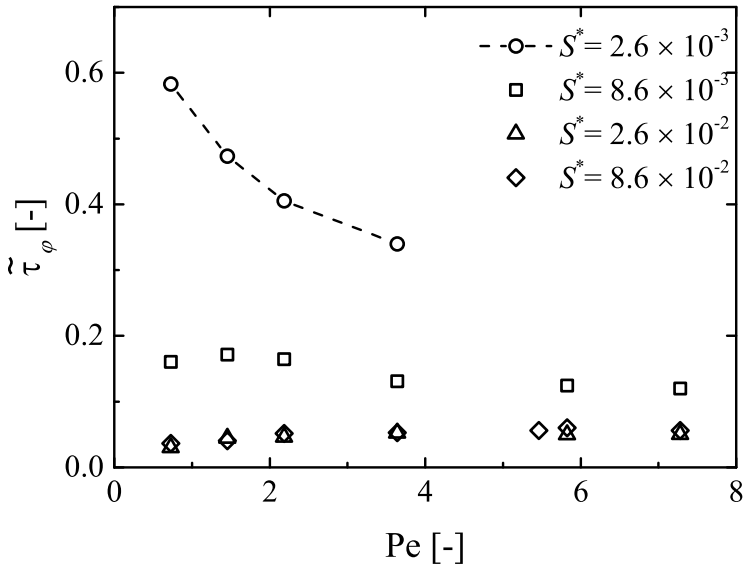

FIG. 10. Relaxation time of the particle volume-fraction, $\tilde{\tau}_\varphi$, as a function of Pe for permeable particles with $\zeta^* = 0.05$, at different particle elastic-softness S^*. For impermeable particles $\tilde{\tau}_\varphi \to \infty$. Prior to shearing, the density of these systems is $\varphi_{\text{free}} = 0.850$ ($n = 1.3 \times 10^{19}$ m^{-3}). Dashed lines connect data points corresponding to simulations shown in Fig. 3.

C. Effect of microscopic dynamics on the stress-relaxation process

This section aims at identifying the microscopic origin of stress relaxation. This is achieved in the following by comparing the different microscopic relaxation mechanisms involved in the process. These are the relaxation of the particle size and the relaxation of the particle position, to the macroscopic stress relaxation.

We have identified the macroscopic stress relaxation in Section IV using the relaxation time $\tilde{\tau}_\sigma$, while the microscopic particle dynamics are described in Section V using $\tilde{\tau}_{\mathrm{MSD}}^{\mathrm{cage}}$ and $\tilde{\tau}_{\mathrm{MSD}}^{\mathrm{esc}}$ for the particle position, and $\tilde{\tau}_\varphi$ for the particle size. Figure 11 shows all time scales described in previous sections for permeable-particle systems with different S^*. Comparing the microscopic relaxation times with the macroscopic stress relaxation, we see consistently for all four systems modeled that the time at which the particles move within their cages $\tilde{\tau}_{\mathrm{MSD}}^{\mathrm{cage}}$ is shorter than the stress relaxation time $\tilde{\tau}_\sigma$, while the time for cage escape, $\tilde{\tau}_{\mathrm{MSD}}^{\mathrm{esc}}$, is significantly longer than the stress relaxation time. These observations lead to the following conclusion. The motion of the particles within their cages is responsible primarily for stress relaxation rather than cage escape or particle-size change. It is noteworthy that both cage rattling and cage escape events have been found to be essential for the crystallization process of systems of hard particles where crystallization is favorable [17]. Crystallization is likewise favorable for the jammed systems of interest for the present work, in particular, they have a favorable crystalline state of FCC [7], which occurs at longer time scales.

Furthermore, we find that the volume fraction relaxes on time scales longer than the stress relaxation times. This shows that stress relaxation occurs while the system is still at the lowest volume fraction reached due to the applied pre-shear (see, for example, Fig. 9). During pre-shear, the particles reduce their volume to accommodate the contact forces. For a certain pre-shear, the stresses in permeable-particle systems relax while the systems is at lower volume fraction than the volume fraction of the impermeable-particle systems with the same elastic properties. It is noteworthy that, at low Péclet number for systems with high particle softness, the relaxation time for the volume fraction is shorter than the relaxation time for the stress. As mentioned earlier, the quality of the integral calculation is lowest at low Pe, because the change in volume fraction between $\tilde{t} = 0$ and longer times is of the same order as the fluctuations.

To elucidate the effect of the volume changes sustained during pre-shear on the stress

relaxation, we show, in Fig. 12, the variation in volume fraction over time of a system with low particle modulus at different pre-shear conditions. Figure 12 shows that at a pre-shear Pe = 72.80 the system at the start of pre-shear was initially at a volume fraction of 0.850 while at the start of flow cessation the volume fraction is 0.720 which is below the close-packing limit of hard spherical particles that is 0.74. At low volume fractions, particles are less constraint by the particles forming the cage, making the cage less effective. Consequently, the stress relaxes faster for permeable-particle systems that are strongly pre-sheared. This section shows an additional aspect of the stress-relaxation dependence on the flow history. In addition to the fact that the pre-shear stress values depend on the applied flow (see Fig. 3), the volume fraction of the system at the start of flow cessation depends on the applied pre-shear.

The results presented in Fig. 11 in view of the system volume fraction upon flow cessation can also be connected to the particle diffusivity. Since stress relaxation is governed by the particle rattling within its cage, as explained earlier, the diffusivity over short time scales, i.e. the short-time diffusion coefficient, is of interest. The short-time diffusion coefficient decreases as the system density increases; this has been shown for hard-particle systems [14, 17, 18] and for permeable-particle systems [7]. More importantly, it is shown in [7] that the short-time diffusion coefficient is larger for permeable particles than impermeable particles for the same free volume fraction. The sustained compression of permeable particles allows them to diffuse more over short times. Since sheared permeable-particle systems are lower in volume fraction than their impermeable counterparts (see Figs. 9, 12), their cages are less effective and they can diffuse more within their cages. Consequently, they exhibit accelerated stress relaxation.

VI. CONCLUSIONS

In this paper, the stress relaxation of jammed suspensions of spongy, permeable particles upon flow cessation is studied in detail. In addition to their ability to impinge, spongy particles are endowed with the ability to undergo volume changes in response to applied deformation or steric effects. Their structure can take up (or expel) the viscous suspending solvent leading to swelling (or shrinking) of particles. To capture the volume changes, one needs to account for the particle size as an independent degree of freedom. In this paper,

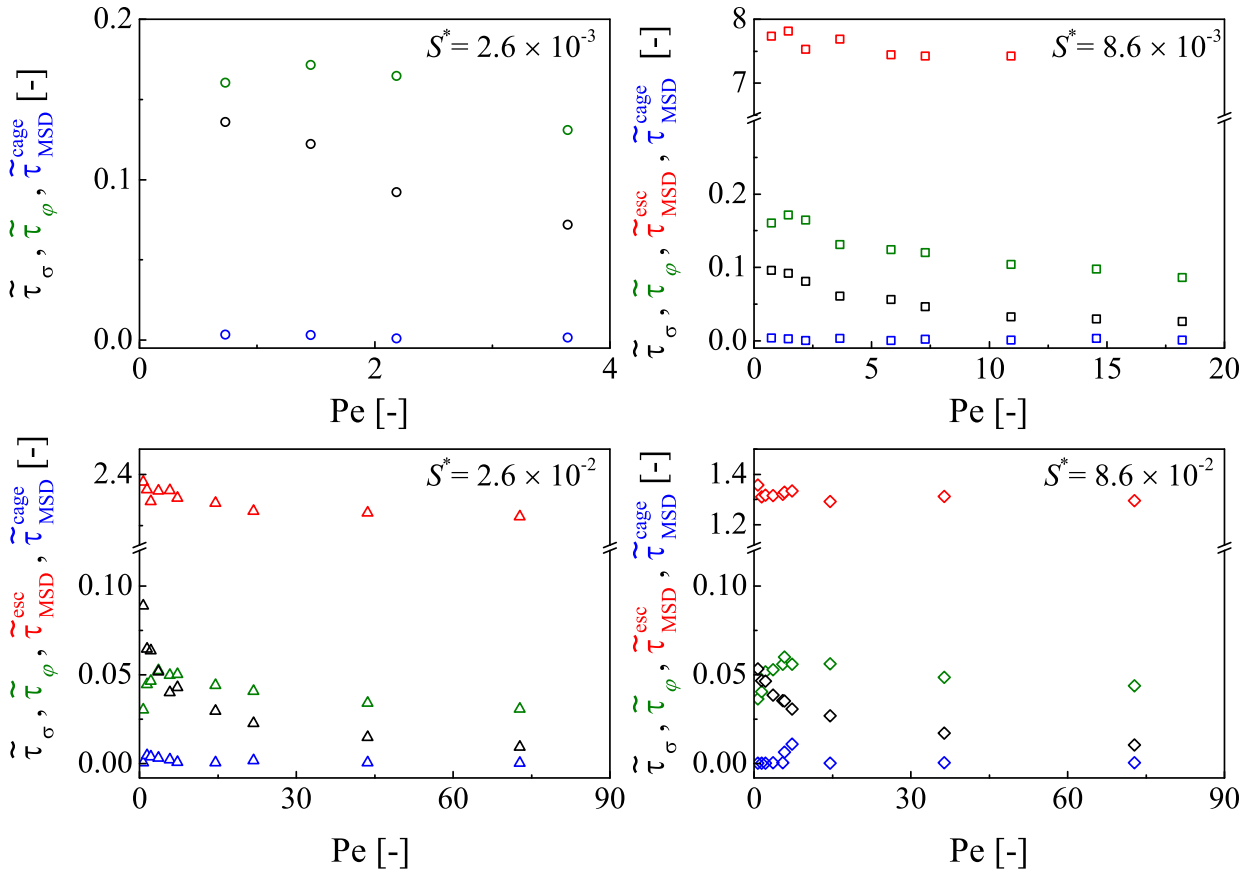

FIG. 11. Different relaxation time of permeable-particle systems $\zeta^* = 0.05$ as a function of Pe with different particle elastic-modulus. The initial density of these systems is $\varphi_{\text{free}} = 0.850$ ($n = 1.3 \times 10^{19}$ m^{-3}).

the application of the dynamic two-scale model developed by Hütter et al. [38] has been extended to suspensions of spongy particles. Simple-shear deformation is applied for a period of time to different particle systems, then switched off at $\tilde{t} = 0$, from which point on we follow the shear-stress relaxation over time. This paper studies the effect of the additional particle degree of freedom, i.e. their size, on the stress relaxation process. So doing, the effect of the particle permeability and the particle elasticity can be studied independently, which is not easily achieved in experiments nor with most of the currently available models.

The main results of the present work are summarized as follows. On the one hand, we find that the macroscopic stress relaxes rapidly after flow cessation to a stress value known as the internal stress which decays, in turn, at a slower rate. For most of our simulations, the internal stress is found to be two orders of magnitude smaller than the pre-shear stress. The

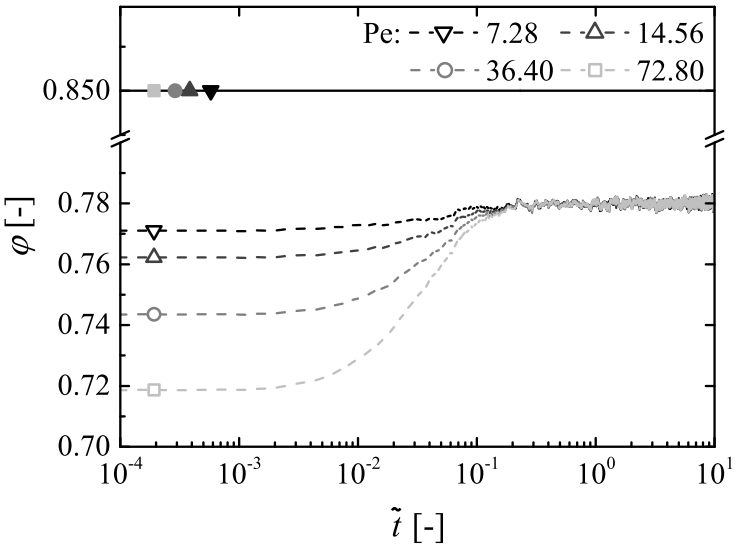

FIG. 12. Particle volume-fraction, φ, over time for an impermeable-particle system (solid line) with $\zeta^* = 0$ and a permeable particle system (dashed lines) with $\zeta^* = 0.05$ and $S^* = 8.6 \times 10^{-2}$ for both systems. The initial density of these systems is $\varphi_{\text{free}} = 0.850$ ($n = 1.3 \times 10^{19}$ m^{-3}).

stress relaxation of suspensions at different pre-shear deformation, particle elastic-softness, and permeability, is studied. The stress relaxation is found to occur faster in the following cases: (i) at higher pre-shear values for a given permeability and particle elastic-softness (see Fig. 5, e.g., dashed line), (ii) for particles with higher elastic-softness at a given particle permeability and applied pre-shear (see Fig. 5, compare closed symbols at a given Pe, e.g., at Pe = 2.18), and (iii) for permeable particles at a given applied pre-shear and elastic-softness (see Fig. 5). On the other hand, concerning the microscopic dynamics, we find that permeable particles diffuse more, at a given time, than impermeable particles of the same elastic properties subjected to the same pre-shear (see Fig. 6). The particle size is found to relax faster at higher pre-shear values for a given particle elastic-softness (see Fig. 10, e.g., dashed line). The particle-size relaxation also occurs faster for permeable particles with higher elastic-softness at a given pre-shear deformation (see Fig. 10, e.g., at Pe = 2.18).

In order to address the main aim of this paper, we have compared the relaxation time of the macroscopic stress to the different relaxation times of the microscopic variables. We recall that the aim of this work is to identify the effect of the particle dynamics on the stress relaxation. This work shows that the stress relaxation proceeds primarily due to relaxation in particle position within their cage formed by the surrounding particles rather

than cage escape. As stress relaxation occurs at lower volume fractions for permeable-particle systems than impermeable-particle systems (of the same equilibrium size), the cages formed by permeable particles (at low volume fraction) are less effective and particles can move easier within their cages. This, hence, explains why stress relaxation is accelerated for permeable particles than impermeable particles.

This work elucidates that the effect of the flow history is two-fold; (i) the stress at the start of flow cessation increases with increasing the applied pre-shear and, (ii) the volume fraction at the start of flow cessation also depends on the applied pre-shear. Although previous models and experiments have investigated the former in detail, the current work highlights the additional influence of the flow history, that is the evolution of the volume fraction during pre-shear. Upon flow cessation, the stress-relaxation process is accelerated by the permeability of spongy particles, namely due to the sustained volume change that was induced during pre-shear, which renders their cages less effective. Practically, this result would be of particular importance in the preparation of soft particles where centrifugation is used to accelerate the particle extraction process [57]. The centrifugation process introduces flow history to the particles that is manifested as pre-shear stresses and sustained size changes. The mechanical properties of systems of such particles are altered by this flow history, if the introduced stresses are not allowed to relax.

We have shown in this paper the importance of size change on the stress-relaxation in the way it affects the flow history. For future work, it can be interesting to model the shape of the particles explicitly. So doing, one can examine the evolution of the particle shape and the resulting anisotropy over time during shear deformation and stress relaxation.

ACKNOWLEDGMENTS

This work forms part of the research programme of the Dutch Polymer Institute (DPI), project #738.

---

[1] J. B. Thorne, G. J. Vine, and M. J. Snowden. Microgel applications and commercial considerations. *Colloid Polym. Sci.*, 289(5-6):625–646, 2011.

[2] M. Das, H. Zhang, and E. Kumacheva. Microgels: Old materials with new applications. *Annu. Rev. Mater. Res.*, 36:117–142, 2006.

[3] A. Bouchoux, P.-E. Cayemitte, J. Jardin, G. Gésan-Guiziou, and B. Cabane. Casein micelle dispersions under osmotic stress. *Biophys. J.*, 96(2):693–706, 2009.

[4] N. L Thomas. The barrier properties of paint coatings. *Prog. Org. Coat.*, 19(2):101–121, 1991.

[5] A. Fernandez-Nieves, H. Wyss, J. Mattsson, and D.A. Weitz. *Microgel Suspensions: Fundamentals and Applications*. Wiley, Hoboken, NJ, 2011.

[6] S. Adams, W. J. Frith, and J. R. Stokes. Influence of particle modulus on the rheological properties of agar microgel suspensions. *J. Rheol.*, 48(6):1195–1213, 2004.

[7] M. E. A. Zakhari, P. D. Anderson, and M. Hütter. Effect of particle-size dynamics on properties of dense spongy-particle systems: Approach towards equilibrium. *Phys. Rev. E*, 96(1):012604, 2017.

[8] G. Romeo, L. Imperiali, J.-W. Kim, A. Fernández-Nieves, and D. Weitz. Origin of de-swelling and dynamics of dense ionic microgel suspensions. *J. Chem. Phys.*, 136(12):124905, 2012.

[9] M. E. A. Zakhari, M. Hütter, and P. D. Anderson. Effect of particle-size dynamics on flow properties of dense spongy-particle systems. *J. Rheol.*, 62(2):543–557, 2018.

[10] B. J. Ackerson and P. N. Pusey. Shear-induced order in suspensions of hard spheres. *Phys. Rev. Lett.*, 61(8):1033–1036, 1988.

[11] L. B. Chen and C. F. Zukoski. Discontinuous shear thinning in ordered suspensions. *Phys. Rev. Lett.*, 65(1):44–47, 1990.

[12] M. Stieger, P. Lindner, and W. Richtering. Structure formation in thermoresponsive microgel suspensions under shear flow. *J. Phys.: Condens. Matter*, 16(38):S3861–S3872, 2004.

[13] J. Vermant and M. J. Solomon. Flow-induced structure in colloidal suspensions. *J. Phys.: Condens. Matter*, 17(4):R187–R216, 2005.

[14] J. F. Brady. The long-time self-diffusivity in concentrated colloidal dispersions. *J.Fluid Mech.*, 272:109–134, 1994.

[15] J. C. Van der Werff and C. G. De Kruif. Hard-sphere colloidal dispersions: The scaling of rheological properties with particle size, volume fraction, and shear rate. *J. Rheol.*, 33(3):421–454, 1989.

[16] P. N. Segre, O. P. Behrend, and P. N. Pusey. Short-time brownian motion in colloidal suspensions: Experiment and simulation. *Phys. Rev. E*, 52(5):5070, 1995.

[17] W. Van Megen and S. M. Underwood. Glass transition in colloidal hard spheres: Measurement and mode-coupling-theory analysis of the coherent intermediate scattering function. *Phys. Rev. E*, 49(5):4206–4220, 1994.

[18] B. Cichocki and K. Hinsen. Self and collective diffusion coefficients of hard sphere suspensions. *Ber. Bunsenges. Phys. Chem.*, 94(3):243–246, 1990.

[19] D. M. Heyes, P. J. Mitchell, P. B. Visscher, and J. R. Melrose. Brownian dynamics simulations of concentrated dispersions: viscoelasticity and near-newtonian behaviour. *J. Chem. Soc. Faraday Trans.*, 90(8):1133–1141, 1994.

[20] D. Vlassopoulos and M. Cloitre. Tunable rheology of dense soft deformable colloids. *Curr. Opin. Colloid Interface Sci.*, 19(6):561–574, 2014.

[21] T. G. Mason, J. Bibette, and D. A. Weitz. Yielding and flow of monodisperse emulsions. *J. Colloid Interface Sci.*, 179(2):439–448, 1996.

[22] M. Cloitre, R. Borrega, and L. Leibler. Rheological aging and rejuvenation in microgel pastes. *Phys. Rev. Lett.*, 85(22):4819–4822, 2000.

[23] L. Mohan, M. Cloitre, and R. T. Bonnecaze. Build-up and two-step relaxation of internal stress in jammed suspensions. *J. Rheol.*, 59(1):63–84, 2015.

[24] M. Ballauff, J. M. Brader, S. U. Egelhaaf, M. Fuchs, J. Horbach, N. Koumakis, M. Krüger, M. Laurati, K. J. Mutch, G. Petekidis, M. Siebenbürger, Th. Voigtmann, and J. Zausch. Residual stresses in glasses. *Phys. Rev. Lett.*, 110(21):215701, 2013.

[25] E. H. Purnomo, D. van den Ende, S. A. Vanapalli, and F. Mugele. Glass transition and aging in dense suspensions of thermosensitive microgel particles. *Phys. Rev. Lett.*, 101(23):238301, 2008.

[26] W. van Megen and P. N. Pusey. Dynamic light-scattering study of the glass transition in a colloidal suspension. *Phys. Rev. A*, 43(10):5429, 1991.

[27] L. C. E. Struik. *Physical aging in amorphous polymers and other materials*, volume 106. Citeseer, 1978.

[28] D. van den Ende, E. H. Purnomo, M. H. G. Duits, W. Richtering, and F. Mugele. Aging in dense suspensions of soft thermosensitive microgel particles studied with particle-tracking microrheology. *Phys. Rev. E*, 81(1):011404, 2010.

[29] G. R. K. Reddy and Y. M. Joshi. Aging under stress and mechanical fragility of soft solids of Laponite. *J. Appl. Phys.*, 104(9):094901, 2008.

[30] B. M. Erwin, D. Vlassopoulos, M. Gauthier, and M. Cloitre. Unique slow dynamics and aging phenomena in soft glassy suspensions of multiarm star polymers. *Phys. Rev. E*, 83(6):061402, 2011.

[31] L. Cipelletti and L. Ramos. Slow dynamics in glassy soft matter. *J. Phys.: Condens. Matter*, 17(6):R253–R285, 2005.

[32] I. Varga, T. Gilányi, R. Meszaros, G. Filipcsei, and M. Zrinyi. Effect of cross-link density on the internal structure of poly(n-isopropylacrylamide) microgels. *J. Phys. Chem. B*, 105(38):9071–9076, 2001.

[33] H. Senff and W. Richtering. Influence of cross-link density on rheological properties of temperature-sensitive microgel suspensions. *Colloid Polym. Sci.*, 278(9):830–840, 2000.

[34] J. R. Seth, L. Mohan, C. Locatelli-Champagne, M. Cloitre, and R. T. Bonnecaze. A micromechanical model to predict the flow of soft particle glasses. *Nat Mater*, 10(11):838–843, 2011.

[35] L. Mohan, R. T. Bonnecaze, and M. Cloitre. Microscopic origin of internal stresses in jammed soft particle suspensions. *Phys. Rev. Lett.*, 111(26):268301, 2013.

[36] T. Gleim, W. Kob, and K. Binder. How does the relaxation of a supercooled liquid depend on its microscopic dynamics? *Phys. Rev. Lett.*, 81(20):4404–4407, 1998.

[37] R. Roa, E. K. Zholkovskiy, and G. Nägele. Ultrafiltration modeling of non-ionic microgels. *Soft matter*, 11(20):4106–4122, 2015.

[38] M. Hütter, T. J. Faber, and H. M. Wyss. Kinetic model for the mechanical response of suspensions of sponge-like particles. *Farad. Discuss.*, 158(1):407–424, 2012.

[39] A. Fernandez-Nieves and A. M. Puertas. *Fluids, Colloids and Soft Materials: An Introduction to Soft Matter Physics*, volume 7 of *Surface and Interfacial Chemistry*. Wiley, Hoboken, NJ, 2016.

[40] C. L. A. Berli and D. Quemada. Rheological modeling of microgel suspensions involving solid-liquid transition. *Langmuir*, 16(21):7968–7974, 2000.

[41] F. Beer, E. Johnston, and J. DeWolf. *Mechanics of Materials*. McGraw-Hill, New York, 2002.

[42] K. L. Johnson. *Contact Mechanics*. Cambridge University Press, Cambridge, 1985.

[43] J. Bergenholtz, J. F. Brady, and M. Vicic. The non-newtonian rheology of dilute colloidal suspensions. *J. Fluid Mech.*, 456:239–275, 2002.

[44] B. E. Dolata and R. N. Zia. Non-equilibrium pair interactions in colloidal dispersions. *J.*

Fluid Mech., 836:694–739, 2018.

[45] M. Ballauff. Spherical polyelectrolyte brushes. *Prog. Polym. Sci.*, 32(10):1135–1151, 2007.

[46] J. J Crassous, M. Siebenbürger, M. Ballauff, M. Drechsler, O. Henrich, and M. Fuchs. Thermosensitive core-shell particles as model systems for studying the flow behavior of concentrated colloidal dispersions. *J. Chem. Phys.*, 125(20):204906, 2006.

[47] A. Verruijt. *Introduction to Soil Dynamics*. Springer, Berlin, 2010.

[48] J. Mewis and N. J. Wagner. *Colloidal Suspension Rheology*. Cambridge Series in Chemical Engineering. Cambridge University Press, 2012.

[49] H. C. Öttinger. *Beyond Equilibrium Thermodynamics*. Wiley, New York, 2005.

[50] A. W. Lees and S. F. Edwards. The computer study of transport processes under extreme conditions. *J. Phys. C: Solid State Phys.*, 5(15):1921–1929, 1972.

[51] A. Quarteroni, R. Sacco, and F. Saleri. *Numerical Mathematics*, volume 37 of *Texts in Applied Mathematics*. Springer, Berlin, 2010.

[52] L. A. Flanagan, Y.-E. Ju, B. Marg, M. Osterfield, and P. A. Janmey. Neurite branching on deformable substrates. *Neuroreport*, 13(18):2411–2415, 2002.

[53] C. Derec, G. Ducouret, A. Ajdari, and F. Lequeux. Aging and nonlinear rheology in suspensions of polyethylene oxide–protected silica particles. *Phys. Rev. E*, 67(6):061403, 2003.

[54] S. Fritschi, M. Fuchs, and Th. Voigtmann. Mode-coupling analysis of residual stresses in colloidal glasses. *Soft Matter*, 10(27):4822–4832, 2014.

[55] Q. Li, X. Peng, and G. B. McKenna. Long-term aging behaviors in a model soft colloidal system. *Soft Matter*, 13(7):1396–1404, 2017.

[56] R. E. Courtland and E. R. Weeks. Direct visualization of ageing in colloidal glasses. *J. Phys.: Cond. Matter*, 15(1):S359, 2002.

[57] S. B. Jhaveri, D. Koylu, D. Maschke, and K. R. Carter. Synthesis of polymeric core–shell particles using surface-initiated living free-radical polymerization. *J. Polym. Sci. A Polym. Chem.*, 45(9):1575–1584, 2007.